Cell Reports
Physical Science

CellPress
OPEN ACCESS

Article

Chlorine-promoted copper catalysts for CO_2 electroreduction into highly reduced products

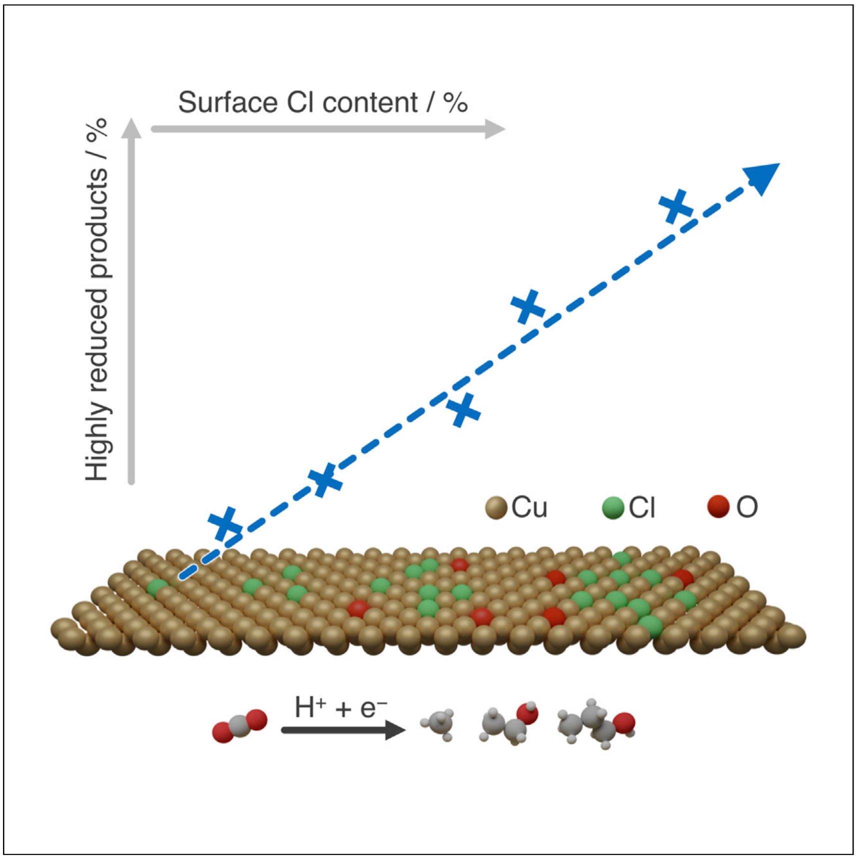

Chlorine modification of copper electrocatalysts can be beneficial for conversion of carbon dioxide selectively into highly reduced products, but poor understanding overshadows the potential to tailor catalysts. Here, Zou and Veenstra et al. reveal how the copper phase and chlorine interact to create a promotional effect, providing design guidelines for copper catalysts.

Tangsheng Zou, Florentine L.P. Veenstra, Enric Ibáñez-Alé, ..., Antonio J. Martín, Núria López, Javier Pérez-Ramírez

jpr@chem.ethz.ch

Highlights

Synthetic procedure to control chlorination treatment of copper electrocatalysts is developed

Mildly chlorinated Cu_2O-based systems are optimal in contrast to Cu and CuO

Surface chlorine content correlates with selectivity toward highly reduced products

Lower barriers toward CH_4 and C_2 product formation are identified on different sites

Zou et al., Cell Reports Physical Science 4, 101294
March 15, 2023 © 2023 The Author(s).
https://doi.org/10.1016/j.xcrp.2023.101294

Please cite this article in press as: Zou et al., Chlorine-promoted copper catalysts for CO_2 electroreduction into highly reduced products, Cell Reports Physical Science (2023), https://doi.org/10.1016/j.xcrp.2023.101294

Cell Reports
Physical Science

CellPress
OPEN ACCESS

Article

Chlorine-promoted copper catalysts for CO_2 electroreduction into highly reduced products

Tangsheng Zou,[1,4] Florentine L.P. Veenstra,[1,4] Enric Ibáñez-Alé,[2,3] Rodrigo García-Muelas,[2] Guido Zichittella,[1] Antonio J. Martín,[1] Núria López,[2] and Javier Pérez-Ramírez[1,5,6,*]

SUMMARY

Chlorinated copper catalysts have shown promise for electroreduction of carbon dioxide to complex products, but the challenging control of chlorination keeps shaded the potential of chlorine as a selectivity promoter. This work develops a gas-phase chlorination strategy based on exposure to diluted hydrochloric acid at different temperatures to study the effect of chlorine content in copper (II) oxide (CuO), copper (I) oxide (Cu_2O), and metallic copper (Cu) foils. Contrary to CuO and Cu, chlorination of Cu_2O enhances the formation of highly reduced products (those requiring more than two electron transfers). Faradaic efficiency toward these products (0%–14% at -0.8 V vs. the reversible hydrogen electrode) correlates with the surface chlorine content after reaction (0 to 1.8 atom % chlorine), which is maximized for mild initial chlorination degrees (Cu_2O:CuCl$\sim$1). Experimental and computational studies suggest metallic copper surfaces with moderate chlorine coverage and oxychloride-like clusters are active sites responsible for the promotional effect. These findings may facilitate structure-performance relationships, forwarding the next generation of this family of catalysts.

INTRODUCTION

The carbon dioxide (CO_2) electroreduction (eCO_2R) toward simple products like carbon monoxide[1] and formate[2] has attracted wider research efforts and more recently the interest of chemical industries. However, more reduced products cannot be generated yet at promising yields under relevant operating conditions, with the single exception of ethylene.[3,4] Besides the initial proof of concept for recently discovered inorganic Ni oxygenates,[5] the only catalysts sustaining more than two proton-electron transfers beyond trace rates[6] are copper-based (Cu-based) materials. However, the tendency of Cu-based electrocatalysts to promote numerous products has driven an intense quest for strategies enabling selectivity control. For this purpose, nanostructure and compositional modifications have been suggested. Early observations[7,8] revealed that halogen-modified catalytic systems display leveraged selectivity toward ethylene, which triggered follow-up efforts to explore their potential.[9] Two strategies based on materials (copper halide catalysts) and electrolytes (halogen-containing) have been practiced so far.

Regarding halogen-containing electrolytes, the positive effect of adding chlorinated, brominated, or iodinated salts like KX (X = Cl, Br, I) to the aqueous medium has been often reported. Most works claim selectivity increases toward

---

[1] Institute of Chemical and Bioengineering, Department of Chemistry and Applied Biosciences, ETH Zürich, Vladimir-Prelog-Weg 1, 8093 Zürich, Switzerland

[2] Institute of Chemical Research of Catalonia, The Barcelona Institute of Science and Technology, Av. Països Catalans, 16, 43007 Tarragona, Spain

[3] Universitat Rovira i Virgili, Avinguda Catalunya, 35, 43002 Tarragona, Spain

[4] These authors contributed equally

[5] Twitter: @catalysis_eth

[6] Lead contact

*Correspondence: jpr@chem.ethz.ch

https://doi.org/10.1016/j.xcrp.2023.101294

This is an open access article under the CC BY-NC-ND license (http://creativecommons.org/licenses/by-nc-nd/4.0/).

C_{2+} products,[10–12] though a few claimed exclusively larger activity toward carbon monoxide.[13,14] In spite of some rationalization efforts, the influence of the halide anion coming from the electrolyte is not well understood, as it is hard to deconvolute from that of its compensating cation, which affects the medium conductivity and double layer structure as well as the CO_2 activation itself.[9,15] Alternatively, copper halide catalysts (CuX, X = Cl, Br, I, with special focus on CuCl) represent the most pursued route through a variety of synthetic strategies, with wet bench methods[16,17] and electrodeposition[8,18–20] being the two most commonly used. Fluorine-containing halides have been less extensively studied.[21,22] Overall, reported C_{2+} Faradaic efficiencies outcompete halogen-free copper systems, reaching up to 80% when operated under optimized conditions,[20,21] though noticeably different performances have been reported over seemingly similar systems.[10,14] It is commonly accepted that copper halides act as catalyst precursors. A common preparation route is exposure of copper halides to reductive potentials to obtain metallic copper matrices with enhanced performance.[8,20,23–25] Alternatively, an intermediate step transforming copper halides into copper oxides has been introduced to increase the population of defects present upon reduction.[17,19] Similarly to the case of modified electrolytes, the role of halogens in the lattice is still unknown, despite pioneering efforts correlating copper halide structures with catalytic performance.[26] Halogen atoms remaining in the copper structure after reconstruction have been proposed to enhance the stability of oxidic Cu centers,[21,22] while other simulations predict that the adsorption of leached halide ions may alter surface electronic properties[20] or hinder the parasitic hydrogen evolution reaction.[9] On the other hand, most reports consider halogens as structure-directing agents toward specific copper facets[17,23] or nanostructures.[18]

In this context, a key pending task is determining synthesis-structure-performance relations linked to the halogenation degree especially for the most widely explored chlorine-based systems. Chlorine exhibits advantageous features compared with bromine, the second most commonly studied halogen to this end. Its more sustainable character and frequent use in industry makes it a preferential target for practical applications. Closely related, bromination of copper phases is much faster than chlorination, making the controlled incorporation of the latter extremely challenging.[27] However, finding a synthetic method enabling controlled chlorination of copper has still remained challenging due to the strong affinity between the two elements, a well-known cause of catalyst deactivation in the Deacon process.[28] As a result, the inability to modulate chlorine content has limited the study of this family of materials to copper chloride, precluding effective catalyst design. This work develops a gas-phase treatment based on exposure to HCl at different temperatures enabling fine control of chlorine incorporation. Partially chlorinated copper systems (Cu, Cu_2O, CuO) were synthesized to reveal a maximal promotion toward highly reduced products (HRPs, i.e., those requiring more than $2e^-$ transfer and comprising CH_4, C_2, and C_3 compounds) for a Cu_2O-based catalyst containing roughly equal Cu_2O and CuCl, underscoring the relevance of selecting the copper phase and chlorination degree. A direct correlation between Faradaic efficiency for HRPs and post-reaction surface chlorine content emerged. Simulations show that the origin of the stability and enhanced performance relies on a large material reconstruction, generating partially chlorinated metallic surfaces and copper oxychloride ensembles showing reduced barriers toward HRPs. These insights thus provide tools and guidelines for the design of enhanced chlorine-promoted copper catalysts.

Please cite this article in press as: Zou et al., Chlorine-promoted copper catalysts for CO_2 electroreduction into highly reduced products, Cell Reports Physical Science (2023), https://doi.org/10.1016/j.xcrp.2023.101294

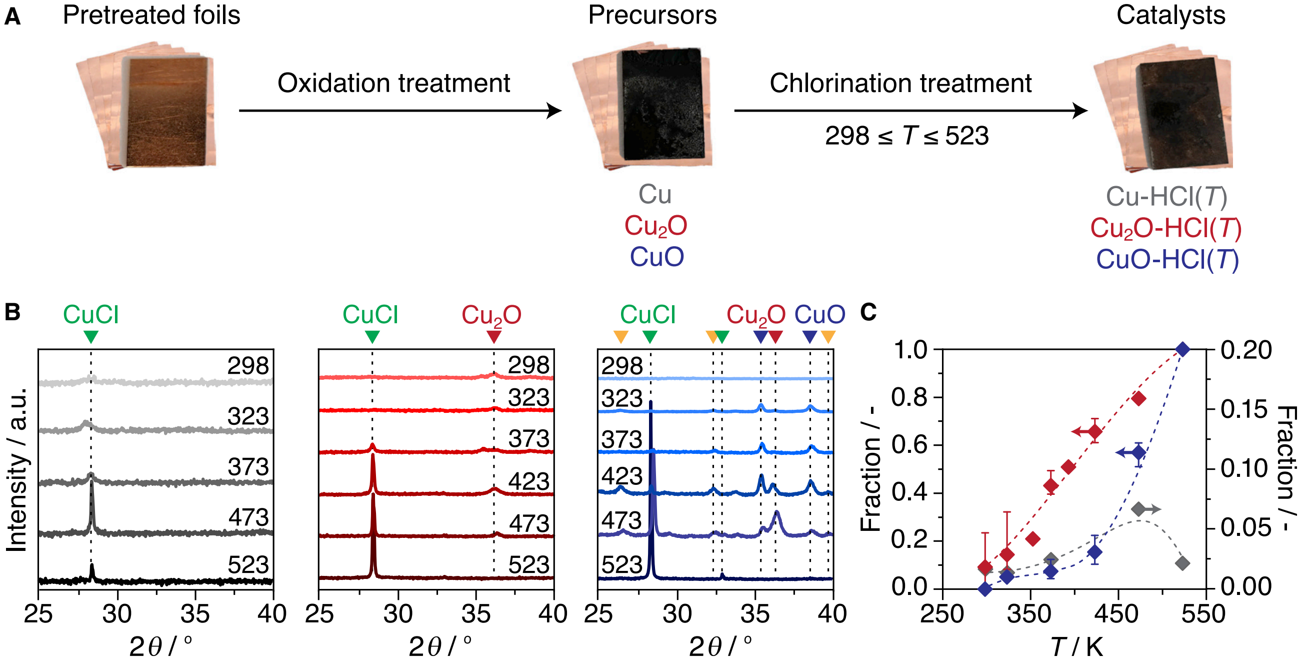

Figure 1. Controlled chlorination of Cu phases

(A) Illustration of the catalyst preparation procedure. Controlled oxidation is followed by halogenation at different temperatures (see Table S1) to achieve different chlorination degrees in the Cu-HCl(*T*), Cu_2O-HCl(*T*), and CuO-HCl(*T*) catalyst series.

(B) XRD profiles of representative fresh Cu-HCl(*T*) (gray), Cu_2O-HCl(*T*) (red), and CuO-HCl(*T*) (blue) catalysts, with indicated chlorination temperatures (in K). Reference peaks are indicated by colored marks, and yellow marks denote metastable phases (see Figure S3).

(C) Bulk variation with chlorination temperature of the fractional abundance of CuCl relative to that of (CuO_x + CuCl) for freshly chlorinated Cu_2O-HCl(*T*), and CuO-HCl(*T*) catalysts, and relative to that of Cu for Cu-HCl(*T*) catalysts. Error bars represent the SD obtained from at least four different electrodes. Color scheme follows that of (B). Phase abundance was determined from XRD profiles as described in the supplemental experimental procedures.

RESULTS AND DISCUSSION

Controlled chlorination of copper catalysts

The first step toward copper catalysts with controlled degree of chlorination was to develop two oxidation treatment protocols (Figure 1A, conditions in Table S1) to obtain bulk Cu_2O or CuO starting from Cu foils. The reason for targeting the two oxidic phases is their different reactivities toward HCl due to the mechanism of lattice O-HCl interaction in the gas phase.[29] Exposure of pretreated Cu foils to the harsher oxidation conditions of 50 vol % O_2/He at 673 K for 30 min was sufficient to predominantly form surface CuO domains as indicated by the presence of (002) and (111) reflections at 35.6° and 38.8° 2θ respectively in the X-ray diffraction (XRD) profiles (Figure S1), in addition to small traces of partially oxidized Cu_2O(111) at 36.7° 2θ. Milder exposure to 20 vol % O_2/He at 553 K for 5 min formed primarily surface Cu_2O as well as traces of over-oxidized CuO domains, as indicated by the Cu_2O(111) reflection at 35.6° 2θ shifting toward lower angles compared with the reference due to lattice strain (Figure S1).

Preliminary tests suggested temperature as the variable enabling better control of the chlorination degree. Chlorination treatment of clean Cu and CuO_x in 2 vol % HCl/He for 30 min at various temperatures resulted in systems with variable copper chlorides content, most notably CuCl as indicated by the (111) reflection at 28.6° 2θ in the XRD profiles of chlorinated samples (Figure 1B). So-prepared samples are coded according to the initial copper phase and chlorination temperature CuO_x-HCl(*T*). While the relative proportion of bulk chloride to oxide phases steadily increases with *T* for Cu_2O-HCl(*T*) (Figure 1C), two distinct regimes are observed for CuO-HCl(*T*), separated by the onset temperature of approximately 450 K, above which copper oxychloride phases form (Figures S2 and S3). Full chlorination of both oxides occurs above 523 K. The overall low bulk CuCl content in the Cu-HCl(*T*) family does not display a strong correlation with chlorination temperature, corroborating the less marked reactivity of the metallic phase. The relative proportion of surface Cl quantified using X-ray photoelectron spectroscopy (XPS) Cl 2*p* signals (Table S2 and Figure S4) followed the general trend in the bulk chlorination degree of the freshly chlorinated CuO-HCl(*T*) and Cu_2O-HCl(*T*) systems. Similarly, assignment of the most intense Cu *LMM* Auger signals for Cu_2O-HCl(*T*) identified a relative decrease and increase of Cu_2O and CuCl, respectively, with increasing chlorination temperature (*vide infra*).

Enhanced performance toward highly reduced products on Cl-promoted Cu_2O systems

Once the set of copper catalysts with controlled chlorination degrees was available, their catalytic performance was evaluated in a two-compartment cell containing CO_2-saturated 0.1 M $KHCO_3$ at −0.8 V vs. RHE, a mild potential at which complex products are not favored on the reference metallic Cu surface.[30] Extended details can be found in the supplemental experimental procedures.

Figure 2 displays product distributions ordered by chlorination temperature for the three catalyst families (see Tables S3–S5 for numerical values and Figure S5 for a typical chronoamperometry profile). Figure 2A reveals that the reference family Cu-HCl(*T*), showing a low and uniform chlorination degree (Figure 1C), displayed a very mild promotional effect. Formate production was slightly enhanced at most temperatures with no discernible pattern. Modest ethylene formation was observed around Cu-HCl(323), aligned with reports claiming enhanced ethylene production on copper halide surfaces.[9] The set of CuO-HCl(*T*) catalysts yielded Faradaic efficiencies toward HRPs seemly independent from the chlorination temperature and similar to that of unmodified CuO, as can be seen in Figure 2B. Faradaic efficiency toward simple compounds, and especially to formate, was favored at intermediate chlorination temperatures. Contrary to the case of metallic copper, the CuCl content varied from 0 to 100% in this set of samples (Figure 1C), suggesting that the initial chlorination degree of CuO-based systems does not influence the ability of the catalyst to produce HRPs.

A different picture emerged for the case of Cu_2O-HCl(*T*) catalysts. Pristine Cu_2O exhibited predominant formation of carbon monoxide and formate with only trace HRPs. Formate production was sharply favored for the Cu_2O-HCl(323) sample. As chlorination temperature rises, HRPs become increasingly predominant up to Cu_2O-HCl(373), for which HRP Faradaic efficiency peaks (ca. 14%, Figure 2A). Of note, production of all compounds gathered under the HRP acronym (methane, C_2 and C_3) increase with chlorination temperature, though the surge of methane must be highlighted. At higher chlorination temperatures the promotional effect is still observable, though to a lesser extent, and it becomes approximately temperature independent. According to the quasi-linear CuCl content-temperature dependence registered for Cu_2O (Figure 1C), this result hinted to an optimized CuCl content of ca. 40% in the system prior to testing. The survey of other potentials suggested that the promotional effect was optimal at potentials around −0.8 V vs. RHE (Table S6), arguably due to the insufficient overpotential available at less cathodic potentials, as well as the likely instability of adsorbed Cl at highly cathodic potentials. Additional experiments upon bromination at room temperature of Cu_2O

Please cite this article in press as: Zou et al., Chlorine-promoted copper catalysts for CO_2 electroreduction into highly reduced products, Cell Reports Physical Science (2023), https://doi.org/10.1016/j.xcrp.2023.101294

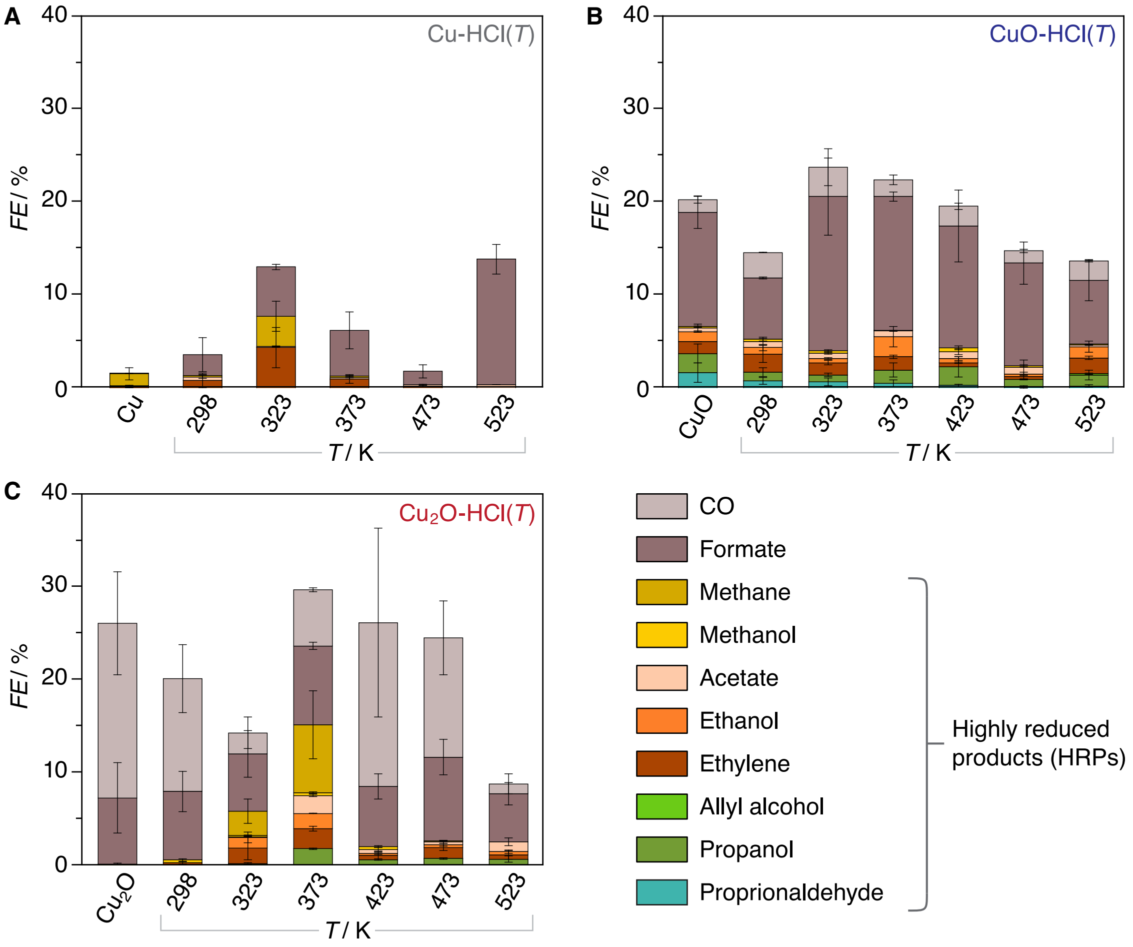

Figure 2. Catalytic performance of chlorine-promoted copper catalysts

(A–C) Faradaic efficiencies toward all detected products in eCO_2R for (A) Cu-HCl(*T*), (B) CuO-HCl(*T*), and (C) Cu_2O-HCl(*T*) electrodes as a function of the chlorination temperature, showing a favorable effect toward formation of highly reduced products (i.e., those requiring more than $2e^-$ transfers) in the case of Cu_2O-HCl(*T*). Hydrogen accounted for the remaining Faradaic efficiencies up to charge balance closing. Reaction conditions: −0.8 V vs. RHE for 50 min in CO_2-saturated 0.1 M $KHCO_3$. Error bars represent the SD of at least two independent measurements.

and CuO shown in Figure S6 disclosed a milder promotional effect toward HRPs than their chlorinated counterparts showing similar degree of halogenation, reinforcing the interest of chlorine promotion.

These distinctive behaviors already disclosed the relevance of the copper source, and that complete chlorination may not be associated with optimal promotional effect in copper materials. The next sections are devoted to elucidating the effect of chlorine on the materials' physico-chemical properties and developing mechanistic insights supporting observed patterns.

Correlation between surface chlorination degree and performance

The first step was to investigate the influence on the promotional effect of surface morphologies introduced by the different synthesis conditions of the catalysts. Differences in surface roughness, which may impact the local chemical environment and thus selectivity,[3,31] were visualized by scanning electron microscopy (SEM, Figure 3A). Micrographs of CuO-HCl(*T*) and Cu_2O-HCl(*T*) catalyst surfaces chlorinated at low, moderate, and high temperatures did not show notably different microscale

Please cite this article in press as: Zou et al., Chlorine-promoted copper catalysts for CO_2 electroreduction into highly reduced products, Cell Reports Physical Science (2023), https://doi.org/10.1016/j.xcrp.2023.101294

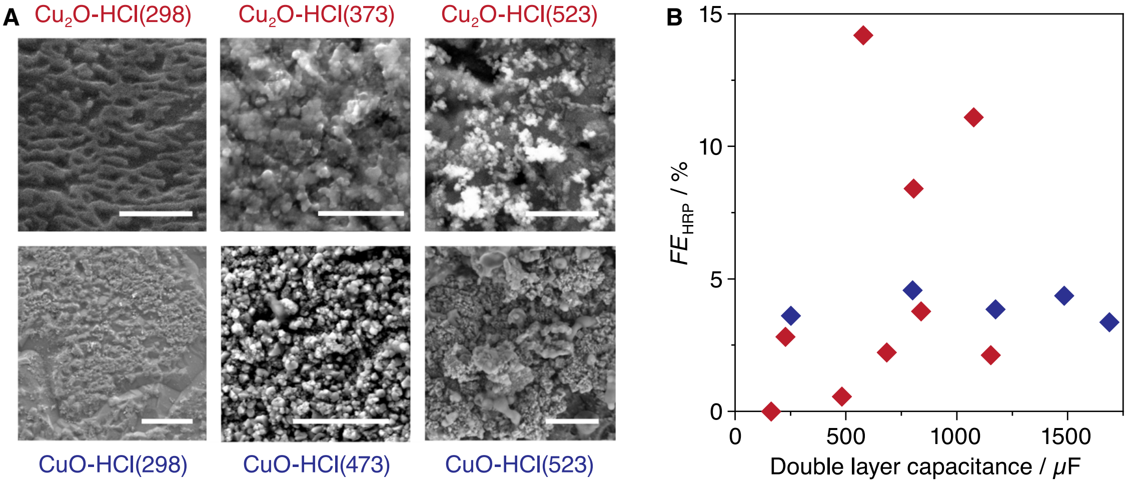

Figure 3. Catalytic performance and surface roughness

(A) SEM micrographs after eCO_2R of representative CuO-HCl(*T*) and Cu_2O-HCl(*T*) electrodes chlorinated at low (298 K), intermediate (373 K and 473 K), and high (523 K) temperatures. Scale bar represents 4 μm.

(B) Faradaic efficiency toward HRPs on Cu_2O-HCl(*T*) (red) and CuO-HCl(*T*) (blue) electrodes as a function of the double-layer capacitance, showing no significant correlation between performance and electrode roughness.

features. In parallel, changes in electrochemically active surface area quantified from double-layer capacitance measurements did not show any discernible correlation with FE_{HRP} (Figure 3B). Since surface morphology may not be a decisive factor explaining the promotional effect, the distinctive trends observed between the three catalyst families may exhibit a chemical ground. Predictably, the density of defects, such as undercoordinated atoms or grain boundaries, or the relative population of facets could also have a relevant role to determine differences in catalytic performance among these systems. Due to the highly dynamic nature of copper surface under operation conditions,[25] its *operando* monitoring would be required, which still represents an experimental challenge. For the case of porous materials like catalytic layers in gas diffusion electrodes, a parallel study considering porosity should be considered.

The concentration and nature of chlorinated species at the reaction interface, which evolved from the fresh structure upon exposure to eCO_2R reaction conditions, were primarily analyzed and quantified using XPS and Auger signals of relevant Cl and Cu regions of used catalyst samples. For all CuO-HCl(*T*) and Cu_2O-HCl(*T*) catalysts, small but quantifiable amounts of Cl reaching up to ca. 0.7 atom % and 1.8 atom %, respectively, remained after reaction (Figures 4A and S7). For Cu_2O-HCl(*T*), a narrow range of temperature with increasing values around the maximum at 373 K for both FE_{HRP} (Figure 2) and surface Cl content (Figure 4B) is evident, suggesting that the choice of treatment temperatures crucially affects both inter-linked phenomena. These observations are combined in Figure 4C, where an apparent linear correlation between FE_{HRP} and surface Cl content is shown for the Cu_2O-HCl(*T*) family.

Note that the dependences of the Cl content with chlorination temperature in fresh (Figure 1C and Table S2) and used materials (Figure 4B) are notably different. Indeed, mild initial chlorination degrees are associated with the largest capability of retaining Cl during reaction. Cu *LMM* Auger spectra of fresh materials (Figure 5A) show the expected increase of the CuCl signal with temperature. Fresh Cu_2O-HCl(373) exhibits comparable intensities for both Cu_2O and CuCl, in line with XRD

Please cite this article in press as: Zou et al., Chlorine-promoted copper catalysts for CO_2 electroreduction into highly reduced products, Cell Reports Physical Science (2023), https://doi.org/10.1016/j.xcrp.2023.101294

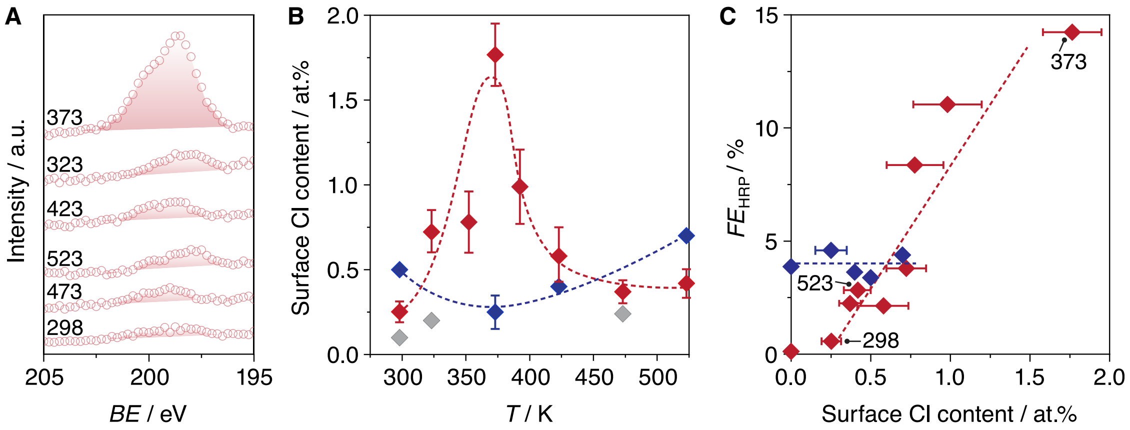

Figure 4. Correlation of catalytic performance with surface Cl content

(A) XPS spectra around the Cl 2*p* region for representative Cu_2O-HCl(*T*) electrodes after eCO_2R, ordered according to the relative abundance of Cl from bottom to top. Areas considered for Cl quantification are shaded. The corresponding analysis for CuO-HCl(*T*) and Cu-HCl(*T*) can be found in Figure S6.

(B) Variation of surface chlorine content after eCO_2R as determined by XPS analysis with chlorination temperature, for Cu_2O-HCl(*T*) (red), CuO-HCl(*T*) (blue), and Cu-HCl(*T*) (gray) electrodes. Error bars represent the SD obtained at three different spots in two different electrodes. Lines are added to guide the eye.

(C) *FE* toward HRPs on Cu_2O-HCl(*T*) and CuO-HCl(*T*) electrodes as a function of surface Cl content after eCO_2R. Error bars represent the SD obtained at three different spots in two different electrodes. Dashed lines have been added to guide the eye, suggesting a promotional effect for Cu_2O-HCl electrodes as the Cl surface content increases. Chlorination temperatures in K have been added next to representative points for Cu_2O-HCl(*T*).

analysis (Figure 1C). After eCO_2R, metallic Cu is the predominant species with small shoulders assigned to CuCl appearing upon increased sputtering time of the samples. Only Cu_2O-HCl(373) features stronger signals pertaining to CuCl and Cu_2O, suggesting that the presence of both phases leads to a distinct (sub)surface state upon exposure to reaction conditions. However, the detection of Cu_2O formed during the exposure of the sample to air cannot be discarded at this point. The surface analysis was complemented by XRD observations (Figure 5B). Since no reflections could be assigned to CuCl in Cu_2O-HCl(*T*) after reaction, it is reasonable to expect that Cl is present as part of smaller surface and subsurface domains without crystalline order or strongly adsorbed on the surface. We thus postulated that *in situ* reduction of Cu oxide and chloride results in the stabilization of Cl around the reduced, defective oxidic surface ensembles formed during eCO_2R,[3] which we denote in general as "copper oxychloride-like ensembles."

The parallel analysis for CuO-HCl(*T*) and Cu-HCl(*T*) catalysts showed different results. They exhibited a very mild dependence of surface Cl content after reaction with chlorination temperature (Figure 4B), with FE_{HRP} largely unchanged compared with their untreated counterparts (Figure 2), leading to no performance-Cl content correlation (Figure 4C). Despite the clear formation of copper chloride and oxychloride phases in the bulk of the used samples that left detectable crystallites as measured by XRD for CuO-HCl(423) and CuO-HCl(473) (Figure 5B), the surface Cl content kept fairly constant around 1 atom % (Figure 4B). This suggests that most of the Cl could be locked in bulk chloride-containing phases outside the XPS measurement depth. The nature of such species and that of surface "copper oxychloride-like ensembles" would conceivably be different for the CuO-HCl(*T*) family, as reflected by their selectivity patterns.

Overall, these results suggest structural differences among families upon exposure to reaction conditions (Figure 5C). For Cu-HCl(*T*), the low Cl content initially incorporated may lead to very sparse Cl coverage after reaction with no significant effect on

Please cite this article in press as: Zou et al., Chlorine-promoted copper catalysts for CO_2 electroreduction into highly reduced products, Cell Reports Physical Science (2023), https://doi.org/10.1016/j.xcrp.2023.101294

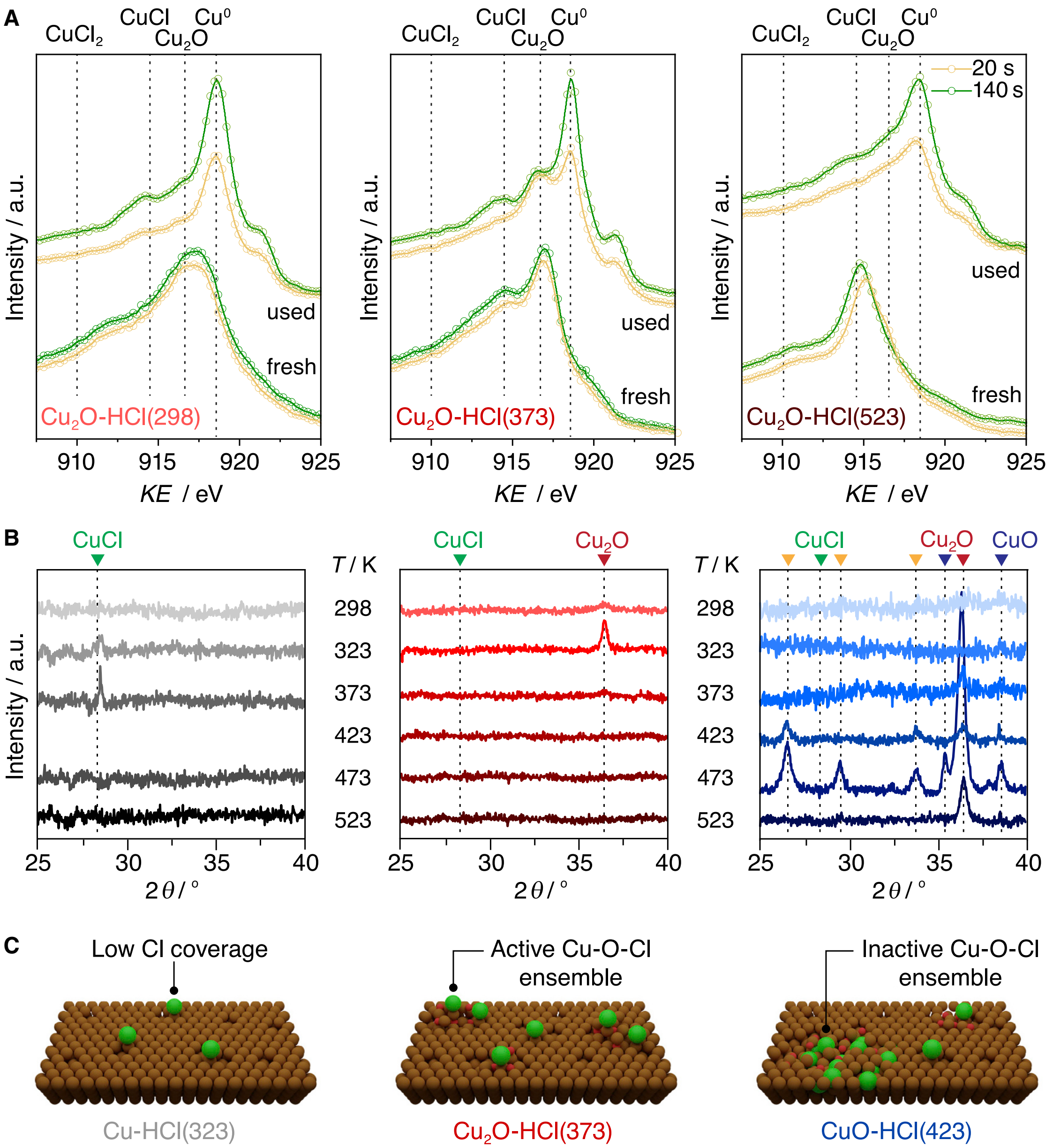

Figure 5. Surface state of chlorinated copper catalysts after eCO_2R

(A) Cu $L_3M_{4,5}M_{4,5}$ Auger lines for fresh and used Cu_2O-HCl(298), Cu_2O-HCl(373), and Cu_2O-HCl(523) catalysts, after surface sputtering for the indicated durations.

(B) XRD profiles of Cu-HCl(*T*), Cu_2O-HCl(*T*), and CuO-HCl(*T*) after eCO_2R with chlorination temperatures (in K) indicated. Full profiles of fresh and used catalysts are shown together in Figure S2. Reference peaks are indicated by colored marks, and yellow marks denote metastable phases (see Figure S3).

(C) Schematic depiction of oxide- and chloride-containing domains at the surface and subsurface of a representative catalyst of each of the three copper electrode families after reaction, showing their distinct natures impacting FE_{HRP}.

HRP formation. For CuO-HCl(*T*), stabilization of inactive subsurface (oxy)chlorides may be responsible for the lack of promotion effect toward HRPs. Finally, for Cu_2O-HCl(*T*), moderate initial chlorination degrees and subsequent exposure to eCO_2R conditions favor higher Cl contents that may be stabilized at the defective, oxygen-containing copper matrix with distinctive electronic features for HRP formation. The combination of the optimum Cu phase and the accuracy of the chlorination procedure are thus crucial.

Please cite this article in press as: Zou et al., Chlorine-promoted copper catalysts for CO_2 electroreduction into highly reduced products, Cell Reports Physical Science (2023), https://doi.org/10.1016/j.xcrp.2023.101294

Identification of active sites and mechanistic investigations

Density functional theory (DFT) simulations contributed to unravel the structural and compositional features affecting HRP formation. The consensus mechanisms in eCO_2R starts with CO_2 adsorption promoted via electron transfer, followed by protonation to *COOH and a proton-coupled electron transfer to produce water and *CO.[3] From there, CO can either desorb or diverge toward C_1 and C_2 HRP formation. Thus, product distribution toward CO, methane, and C_{2+} products is controlled by the energy of *CO desorption, *CO protonation to *COH, and *CO-CO coupling,[32–34] which are taken as descriptors for selectivity.

The nature of the active sites in native copper catalysts under eCO_2R is controversial due to the deep structural changes depending on the reaction conditions and the initial oxidation state of the material.[35–37] Recent studies[25,38] suggest that the existence of metallic Cu^0, oxidic Cu^+, and polarized $Cu^{\delta+}$ might be responsible for the C-C coupling ability. Similarly to oxygen, chlorine can also act as modifier in similar terms due to their similar electronegativity. Therefore, the ability to present variable oxidation states in the chlorinated materials may be a favorable feature for enhancing reactivity.

Thermodynamic properties of relevant intermediates were analyzed on different Cl-modified copper surfaces. First, the stability and electronic properties of metallic copper surfaces showing increasing chlorine coverages was explored considering the desorption of chlorine atoms on the lowest surface energy facets Cu(111), Cu(100), and Cu(110),[39] as well as on Cu(211) step models. Although electrolyte-metal interface studies[40] have shown the key role of halide adlayers on Cu surfaces, they might be modestly stable under eCO_2R conditions.[41] However, these structures constitute the simplest model to understand the electronic effect exerted by Cl on its nearest Cu atoms. Given the maximum XPS-derived Cl coverage of ca. 0.20 ML after reaction (Figure 4),[42] simulations covered the 0.00–0.33 ML range at −0.80 V vs. RHE with implicit solvation. The results on Cu(100) show that chlorine desorption energies are independent of coverage within this range (Table S7). Chlorine adatoms on Cu(100) are marginally stable (Tables S8 and S9) since desorption as aqueous Cl^- is close to thermoneutrality ($\Delta G_{des} = -0.23$ eV, $U = -0.80$ V vs. RHE), similar to the case of Cu(110) and Cu(211) ($\Delta G_{des} = -0.21$ eV and -0.13 eV, respectively), while Cl^- on Cu(111) is even less stable ($\Delta G_{des} = -0.54$ eV). Desorption energies of Cl from Cu(100) and *ab initio* thermodynamics-derived adsorption energies per unit area (Figure S8) both indicate reduced stability at potentials more negative than $U = -0.57$ V vs. RHE. As *Cl-*Cl lateral interactions are negligible, effects of chlorine incorporation are localized, modifying the electronic density of the nearest neighboring Cu atoms as shown by the Bader charge of 0.10–0.15 $|e^-|$ (Figure 6A and Table S10) and supported by *d*-band analyses (Figure S9 and Table S11). Therefore, surface chlorination may generate polarized $Cu^{\delta+}$ species, known to have an important role in eCO_2R.[43,44] As charging creates asymmetric Cu-$Cu^{\delta+}$ pairs and *CO adsorption energy on Cu sites close to Cl atoms is smaller than on regular Cu sites (Figure 6B), the *CO-CO coupling energy is lowered compared with clean Cu without significantly altering other steps, enhancing C_2 HRP formation (Figure 6C). For Cl coverages above 0.17 ML, the decreasing frequency of these pairs diminishes this effect, promoting CO desorption instead (Figure 6B). *H adsorption strength was however found to be unaffected with respect to Cl coverage (Figure S10, $E_{*H,ads} = -0.90$ eV), suggesting that the competing hydrogen evolution reaction remains unaltered. Energy profiles leading to different HRPs (Figures S11 and S12) demonstrate that the applied potential is crucial in achieving C-C bond formation. However, this modification does not lead to enhanced formation of C_1 HRPs (namely methane) (Figures S13–S16).

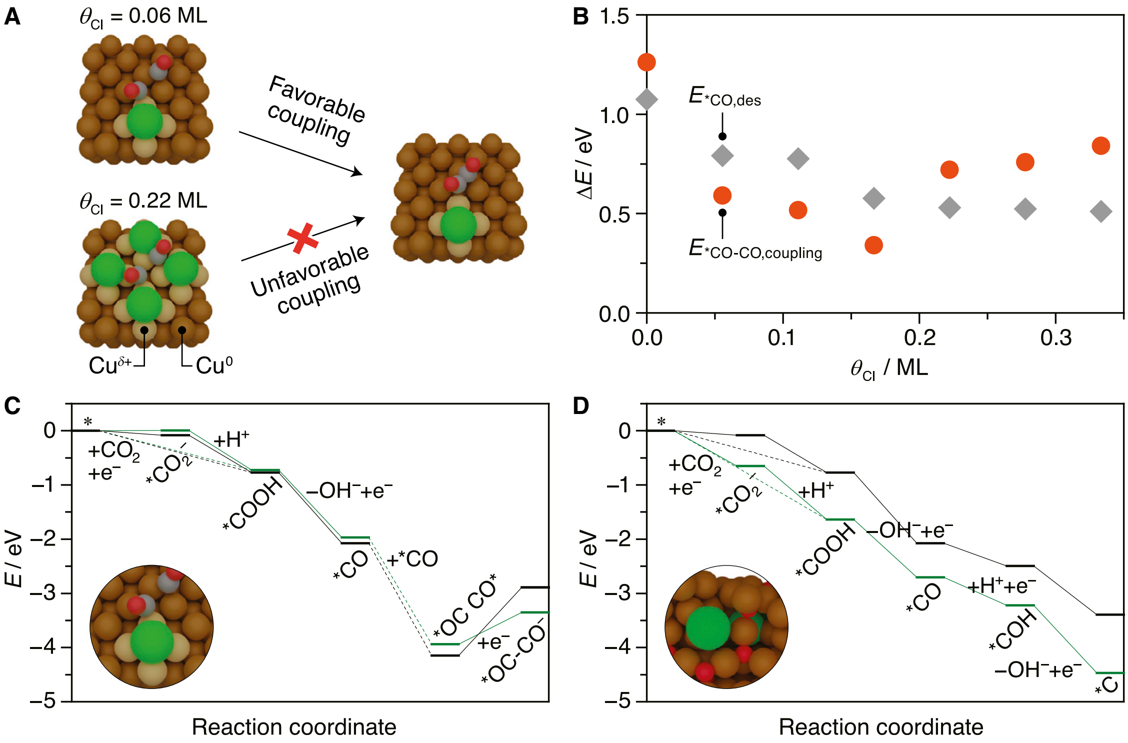

Figure 6. Impact of surface chlorination on the reaction mechanism

(A) Schematic depiction of the effect of Cl adatoms on neighboring copper atoms at the Cu(100) surface for varying Cl coverages, with polarized Cu atoms next to Cl ones (Bader charge = 0.15 |e⁻|) displayed in a lighter color.

(B) Variation of *CO desorption ($E_{*CO,des}$) and *CO-CO coupling ($E_{*CO\text{-}CO\text{-},coupling}$) energies as a function of Cl coverage (θ_{Cl}) on Cu(100).

(C) Energy profile for eCO_2R up to the $*OC\text{-}CO^-$ intermediate at −0.80 V vs. RHE over clean (black) and chlorinated (green, structure depicted, θ_{Cl} = 0.07 ML) Cu(100) surfaces.

(D) Energy profile for eCO_2R up to the *C intermediate at −0.80 V vs. RHE over clean Cu(100) (black) and Cu_2O-Cl (green, structure depicted) surfaces, respectively.

To discover stable structures able to generate asymmetric Cu-$Cu^{\delta+}$ pairs and promote C_1 HRP formation, a heuristic approach involving model systems mirroring the structural complexity resulting from the chlorination treatment protocol was devised. Noting the optimal surface Cl content for Cu_2O-HCl(373) where both oxidic and chloride phases coexisted prior to eCO_2R (Figure 5), a total of 68 structural models representing a wide compositional range were built upon $Cu_2O(111)$ as a reference, with certain oxygen atoms removed and (H)Cl incorporated, to assess stable copper (hydr)oxychloride phases (see supplemental experimental procedures and Figure S17 for full details).[25] All structures were optimized via DFT, and their computed energies were compared with a predicted energy dependent on only the stoichiometry, using a general equation with the form of Equation S21. Multivariate linear regression and subsequent refinement of the variable selection resulted in a final regression model iteration that uses the numbers of Cl, H, and O atoms, as well as *Cl adatoms, as independent variables (see supplemental experimental procedures and Table S12). The independence of variables precluding interaction-dependent terms implies that structures with DFT energies (E_{DFT}) lower than these predicted by the regression model (E_{pred}) show synergetic effects that render them more stable (Figure S18A). The cooperative effects (up to −1.76 eV) appear to be associated with structural motifs that locally resemble Cu_2OCl_2-like (Figure S18B) or CuOHCl-like (Figure S18C) bulk structures.[25]

Please cite this article in press as: Zou et al., Chlorine-promoted copper catalysts for CO_2 electroreduction into highly reduced products, Cell Reports Physical Science (2023), https://doi.org/10.1016/j.xcrp.2023.101294

The stability of these copper (hydroxy)chloride ensembles was ascertained by calculating energies of chlorine desorption to Cl^- for the three most stable structures identified. Over the Cu_2OCl_2-like ensemble, the energy of both subsurface Cl atoms is $\Delta G_{des} = -0.26$ eV at $U = -0.80$ V vs. RHE, and kinetic trapping due to poor Cl^- diffusion to the surface is unlikely (process is endergonic by 0.2 eV). This suggests that Cl atoms are strongly stabilized if ensembles are generated at the surface, as their desorption Gibbs free energy is much higher (1.0–2.5 eV more endergonic) than those of other subsurface Cl atoms in other structures and also higher (0.2–1.5 eV more endergonic) than surface-stabilized Cl atoms (Table S13). Despite the suggested stability of CuOHCl-like ensembles by the heuristic model, the desorption energy of Cl subsurface atoms on the structures ($\Delta G_{des} = -1.27$ eV) suggests their low stability under applied potential. The unique stability of the Cu_2OCl_2-like ensembles mirrors that of their bulk counterparts as detected by XRD (Figure S3) and XPS (Figure 5A) measurements of used CuO-HCl(*T*) catalysts, while CuOHCl initially present disappears under reaction conditions (Figure S3). Cu_2OCl_2-like ensembles induce changes in the neighboring Cu *d*-band centers with respect to Cu atoms located further away, by $\Delta\varepsilon_{d\text{-band}} = 0.32$ eV (Figure S19), in opposition to Cu(100). Moreover, the most stable Cu_2OCl_2-like ensemble showed a significant promotional effect toward CH_4 formation (Figure 6D), as CO_2 adsorption is more favorable by −0.57 eV compared with over Cu(100). Subsequent protonation and dehydroxylation steps leading to *C are also slightly more favored by −0.10 eV and −0.35 eV, respectively, with a stronger CO adsorption by 0.73 eV. Thus, Cu_2OCl_2-like ensembles could be assigned as sites responsible for C_1 HRPs, while for the metastable CuOHCl-like ensembles, no promotion is found (Figure S20). Also, Bader charge analysis demonstrates the generation of surface Cu-$Cu^{\delta+}$ pairs in Cu_2OCl_2-like ensembles able to promote C_{2+} products (Figure S21 and Table S14). From a wider perspective, the nature of herein suggested active sites for the promotion of methane explains why chlorine-modified copper catalysts reported in the literature have exclusively been claimed to favor multi-carbon products. Since all previous reports were based on copper chloride due to lack of a method to control chlorination degree, the virtual absence of oxygen in the initial material precludes the formation of Cu_2OCl_2-like ensembles.

In summary, this work developed a method to control the chlorination degree of copper electrocatalysts and applied it to Cu, CuO, and Cu_2O to investigate structure-performance correlations. Surface chlorine content upon reaction correlates with FE_{HRP} and could be maximized for mildly chlorinated Cu_2O materials, revealing the importance of both the copper phase and the synthesis procedure. This work also reveals the potential of chlorine-promoted copper catalysts for the production of methane. Computational studies predict two types of sites to explain observed performance patterns. Chlorine incorporation both on Cu surfaces and in stable copper oxychloride phases showed that *CO-CO coupling could be enhanced by mild Cl contents giving rise to asymmetric Cu-$Cu^{\delta+}$ pairs with higher reactivity, while methane formation is thermodynamically favored over copper oxychloride-containing structures. These tools and fundamental insights gathered are expected to contribute to the design of the next generation of technical chlorine-promoted copper electrocatalysts.

EXPERIMENTAL PROCEDURES

Resource availability

Lead contact

Further information and requests for resources and reagents should be directed to and will be fulfilled by the lead contact, Javier Pérez-Ramírez (jpr@chem.ethz.ch).

Materials availability

This study did not generate new unique materials.

Data and code availability

Experimental data relating to the figures and tables presented in this manuscript have been deposited at Zenodo under the https://doi.org/10.5281/zenodo.7199360 and are publicly available as of the date of publication. Supporting DFT datasets have been deposited at ioChem-BD[45] under the https://doi.org/10.19061/iochem-bd-1-258 and are publicly available as of the date of publication. This paper does not report original code. Any additional information required to reanalyze the data reported in this paper is available from the lead contact upon reasonable request.

Catalyst preparation

Polished Cu foils were oxidized in a flow of dilute oxygen at tailored conditions, followed by chlorination in a gas flow of 2 vol % hydrogen chloride diluted in helium at temperatures between 298 K and 523 K, to obtain three families of catalysts: Cu-HCl(*T*), Cu_2O-HCl(*T*), and CuO-HCl(*T*). Further details on catalyst preparation are provided in the supplemental experimental procedures with the conditions applied in the oxidation and chlorination treatments fully detailed in Table S1.

Catalyst characterization

XRD analysis was used to identify and quantify bulk phases and investigate their crystallinity. XPS measurements were carried out to identify copper phases and quantify chlorine content. SEM disclosed structural features at the microscale. Further details for each of the characterization techniques are provided in the supplemental experimental procedures.

Catalyst evaluation

Catalyst evaluation was performed in a gas-tight two-compartment cell, mounted with a microporous carbon layer as counter electrode and Ag/AgCl 3 M as reference electrode at −0.8 V vs. RHE in CO_2-saturated 0.1 M $KHCO_3$. On-line gaseous products quantification was performed by gas chromatography every 15 min, whereas liquid products were analyzed by proton nuclear magnetic resonance (^{1}H-NMR) spectrometry after reaction. An extended description can be found in the supplemental experimental procedures.

Theoretical calculations

DFT calculations were performed with the Vienna Ab initio Simulation Package (VASP)[46,47] using the Perdew-Burke-Ernzerhof (PBE) exchange-correlation functional[48] with dispersion included through the DFT-D2 method.[49] Inner electrons were represented through projector augmented wave (PAW) pseudopotentials[50] with a plane-wave energy cutoff of 450 eV. Mechanistic studies were performed on the chlorine adatom and heuristically computed copper (hydr)oxychloride models using the computational hydrogen electrode (CHE) model[51] and solvation.[52] Further details on DFT parameters, model generation, and energy calculations are provided in the supplemental experimental procedures.

SUPPLEMENTAL INFORMATION

Supplemental information can be found online at https://doi.org/10.1016/j.xcrp.2023.101294.

Please cite this article in press as: Zou et al., Chlorine-promoted copper catalysts for CO_2 electroreduction into highly reduced products, Cell Reports Physical Science (2023), https://doi.org/10.1016/j.xcrp.2023.101294

ACKNOWLEDGMENTS

The authors acknowledge financial support from the Swiss National Science Foundation through the National Center of Competence in Research NCCR Catalysis (grant 180544), ETH grant ETH-47 19-1, and from the Spanish Ministry of Science and Innovation (PRE2021-097615, PID2021-122516OB-I00, Severo Ochoa Center of Excellence CEX2019-000925-S 10.13039/501100011033). The Barcelona Supercomputing Centre-MareNostrum (BSC-RES) is acknowledged for providing generous computational resources. T.Z. thanks the Agency for Science, Technology and Research (A*STAR) Singapore for support through a graduate fellowship. The authors thank Thaylan P. Araújo and Dr. Simon Büchele for assistance with XPS measurements and Shibashish Jaydev for assistance with visualizations.

AUTHOR CONTRIBUTIONS

T.Z. and F.L.P.V., methodology, data curation, investigation, visualization, writing – original draft. E.I.-A, data curation, investigation, visualization, writing – original draft. R.G.-M. and G.Z., methodology. A.J.M., methodology, investigation, visualization, validation, supervision, writing – original draft. N.L., conceptualization, funding acquisition, supervision, project administration, writing – review & editing. J.P.-R., conceptualization, funding acquisition, supervision, project administration, writing – review & editing.

DECLARATION OF INTERESTS

The authors declare no competing interests.

Received: November 10, 2022
Revised: December 22, 2022
Accepted: January 25, 2023
Published: February 17, 2023

REFERENCES

1. Gao, F.-Y., Bao, R.-C., Gao, M.-R., and Yu, S.-H. (2020). Electrochemical CO_2-to-CO conversion: electrocatalysts, electrolytes, and electrolyzers. J. Mater. Chem. *8*, 15458–15478.

2. Al-Tamreh, S.A., Ibrahim, M.H., El-Naas, M.H., Vaes, J., Pant, D., Benamor, A., and Amhamed, A. (2021). Electroreduction of carbon dioxide into formate: a comprehensive review. Chemelectrochem *8*, 3207–3220.

3. Nitopi, S., Bertheussen, E., Scott, S.B., Liu, X., Engstfeld, A.K., Horch, S., Seger, B., Stephens, I.E.L., Chan, K., Hahn, C., et al. (2019). Progress and perspectives of electrochemical CO_2 reduction on copper in aqueous electrolyte. Chem. Rev. *119*, 7610–7672.

4. Ioannou, I., D'Angelo, S.C., Martín, A.J., Pérez-Ramírez, J., and Guillén-Gosálbez, G. (2020). Hybridization of fossil- and CO_2 based routes for ethylene production using renewable energy. ChemSusChem *13*, 6370–6380.

5. Zhou, Y., Martín, A.J., Dattila, F., Xi, S., López, N., Pérez-Ramírez, J., and Yeo, B.S. (2022). Long-chain hydrocarbons by CO_2 electroreduction using polarized nickel catalysts. Nat. Catal. *5*, 545–554.

6. Wang, Y., Liu, J., and Zheng, G. (2021). Designing copper-based catalysts for efficient carbon dioxide electroreduction. Adv. Mater. *33*, 2005798.

7. Ogura, K., Yano, H., and Shirai, F. (2003). Catalytic reduction of CO_2 to ethylene by electrolysis at a three-phase interface. J. Electrochem. Soc. *150*, D163.

8. Yano, H., Tanaka, T., Nakayama, M., and Ogura, K. (2004). Selective electrochemical reduction of CO_2 to ethylene at a three-phase interface on copper(i) halide-confined cu-mesh electrodes in acidic solutions of potassium halides. J. Electroanal. Chem. *565*, 287–293.

9. Masana, J.J., Peng, B., Shuai, Z., Qiu, M., and Yu, Y. (2022). Influence of halide ions on the electrochemical reduction of carbon dioxide over a copper surface. J. Mater. Chem. *10*, 1086–1104.

10. Ogura, K. (2013). Electrochemical reduction of carbon dioxide to ethylene: mechanistic approach. J. CO_2 Util. *1*, 43–49.

11. Reller, C., Krause, R., Volkova, E., Schmid, B., Neubauer, S., Rucki, A., Schuster, M., and Schmid, G. (2017). Selective electroreduction of CO_2 toward ethylene on nano dendritic copper catalysts at high current density. Adv. Energy Mater. *7*, 1602114.

12. Gao, D., Scholten, F., and Roldan Cuenya, B. (2017). Improved CO_2 electroreduction performance on plasma-activated Cu catalysts via electrolyte design: halide effect. ACS Catal. *7*, 5112–5120.

13. Schizodimou, A., and Kyriacou, G. (2012). Acceleration of the reduction of carbon dioxide in the presence of multivalent cations. Electrochim. Acta *78*, 171–176.

14. Varela, A.S., Ju, W., Reier, T., and Strasser, P. (2016). Tuning the catalytic activity and selectivity of Cu for CO_2 electroreduction in the presence of halides. ACS Catal. *6*, 2136–2144.

15. Monteiro, M.C.O., Dattila, F., Hagedoorn, B., García-Muelas, R., López, N., and Koper, M.T.M. (2021). Absence of CO_2 electroreduction on copper, gold and silver electrodes without metal cations in solution. Nat. Catal. *4*, 654–662.

16. Wang, J., Yang, H., Liu, Q., Liu, Q., Li, X., Lv, X., Cheng, T., and Wu, H.B. (2021). Fastening br– ions at copper–molecule interface enables highly efficient electroreduction of CO_2 to ethanol. ACS Energy Lett. *6*, 437–444.

17. Kibria, M.G., Dinh, C.-T., Seifitokaldani, A., De Luna, P., Burdyny, T., Quintero-Bermudez, R., Ross, M.B., Bushuyev, O.S., García de Arquer, F.P., Yang, P., et al. (2018). A surface

Please cite this article in press as: Zou et al., Chlorine-promoted copper catalysts for CO_2 electroreduction into highly reduced products, Cell Reports Physical Science (2023), https://doi.org/10.1016/j.xcrp.2023.101294

reconstruction route to high productivity and selectivity in CO_2 electroreduction toward C_{2+} hydrocarbons. Adv. Mater. *30*, 1804867.

18. Han, J., Long, C., Zhang, J., Hou, K., Yuan, Y., Wang, D., Zhang, X., Qiu, X., Zhu, Y., Zhang, Y., et al. (2020). A reconstructed porous copper surface promotes selectivity and efficiency toward C_2 products by electrocatalytic CO_2 reduction. Chem. Sci. *11*, 10698–10704.

19. Kim, T., and Palmore, G.T.R. (2020). A scalable method for preparing Cu electrocatalysts that convert CO_2 into C_{2+} products. Nat. Commun. *11*, 3622.

20. Gao, D., Sinev, I., Scholten, F., Arán-Ais, R.M., Divins, N.J., Kvashnina, K., Timoshenko, J., and Roldan Cuenya, B. (2019). Selective CO_2 electroreduction to ethylene and multicarbon alcohols via electrolyte-driven nanostructuring. Angew. Chem., Int. Ed. Engl. *58*, 17047–17053.

21. Ma, W., Xie, S., Liu, T., Fan, Q., Ye, J., Sun, F., Jiang, Z., Zhang, Q., Cheng, J., and Wang, Y. (2020). Electrocatalytic reduction of CO_2 to ethylene and ethanol through hydrogen-assisted C–C coupling over fluorine-modified copper. Nat. Catal. *3*, 478–487.

22. Li, M., Ma, Y., Chen, J., Lawrence, R., Luo, W., Sacchi, M., Jiang, W., and Yang, J. (2021). Residual chlorine induced cationic active species on a porous copper electrocatalyst for highly stable electrochemical CO_2 reduction to C_{2+}. Angew. Chem., Int. Ed. Engl. *60*, 11487–11493.

23. Chen, C.S., Handoko, A.D., Wan, J.H., Ma, L., Ren, D., and Yeo, B.S. (2015). Stable and selective electrochemical reduction of carbon dioxide to ethylene on copper mesocrystals. Catal. Sci. Technol. *5*, 161–168.

24. Lee, S., Kim, D., and Lee, J. (2015). Electrocatalytic production of C_3-C_4 compounds by conversion of CO_2 on a chloride-induced bi-phasic Cu_2O-Cu catalyst. Angew. Chem., Int. Ed. Engl. *54*, 14701–14705.

25. Dattila, F., García-Muelas, R., and López, N. (2020). Active and selective ensembles in oxide-derived copper catalysts for CO_2 reduction. ACS Energy Lett. *5*, 3176–3184.

26. Wang, H., Matios, E., Wang, C., Luo, J., Lu, X., Hu, X., and Li, W. (2019). Rapid and scalable synthesis of cuprous halide-derived copper nano-architectures for selective electrochemical reduction of carbon dioxide. Nano Lett. *19*, 3925–3932.

27. Winterton, N. (2000). Chlorine: the only green element – towards a wider acceptance of its role in natural cycles. Green Chem. *2*, 173–225.

28. Pérez-Ramírez, J., Mondelli, C., Schmidt, T., Schlüter, O.F.K., Wolf, A., Mleczko, L., and Dreier, T. (2011). Sustainable chlorine recycling via catalysed HCl oxidation: from fundamentals to implementation. Energy Environ. Sci. *4*, 4786–4799.

29. Amrute, A.P., Mondelli, C., Hevia, M.A.G., and Pérez-Ramírez, J. (2011). Temporal analysis of products study of HCl oxidation on copper- and ruthenium-based catalysts. J. Phys. Chem. C *115*, 1056–1063.

30. Kuhl, K.P., Cave, E.R., Abram, D.N., and Jaramillo, T.F. (2012). New insights into the electrochemical reduction of carbon dioxide on metallic copper surfaces. Energy Environ. Sci. *5*, 7050–7059.

31. Veenstra, F.L., Ackerl, N., Martín, A.J., and Pérez-Ramírez, J. (2020). Laser-microstructured copper reveals selectivity patterns in the electrocatalytic reduction of CO_2. Chem *6*, 1707–1722.

32. Birdja, Y.Y., Pérez-Gallent, E., Figueiredo, M.C., Göttle, A.J., Calle-Vallejo, F., and Koper, M.T.M. (2019). Advances and challenges in understanding the electrocatalytic conversion of carbon dioxide to fuels. Nat. Energy *4*, 732–745.

33. Zhan, C., Dattila, F., Rettenmaier, C., Bergmann, A., Kühl, S., García-Muelas, R., López, N., and Cuenya, B.R. (2021). Revealing the CO coverage-driven C–C coupling mechanism for electrochemical CO_2 reduction on Cu_2O nanocubes via operando Raman spectroscopy. ACS Catal. *11*, 7694–7701.

34. An, H., Wu, L., Mandemaker, L.D.B., Yang, S., de Ruiter, J., Wijten, J.H.J., Janssens, J.C.L., Hartman, T., van der Stam, W., and Weckhuysen, B.M. (2021). Sub-second time-resolved surface-enhanced Raman spectroscopy reveals dynamic CO intermediates during electrochemical CO_2 reduction on copper. Angew. Chem., Int. Ed. Engl. *60*, 16576–16584.

35. Popović, S., Smiljanić, M., Jovanovič, P., Vavra, J., Buonsanti, R., and Hodnik, N. (2020). Stability and degradation mechanisms of copper-based catalysts for electrochemical CO_2 reduction. Angew. Chem., Int. Ed. Engl. *59*, 14736–14746.

36. Li, C.W., and Kanan, M.W. (2012). CO_2 reduction at low overpotential on Cu electrodes resulting from the reduction of thick Cu_2O films. J. Am. Chem. Soc. *134*, 7231–7234.

37. Lum, Y., and Ager, J.W. (2018). Stability of residual oxides in oxide-derived copper catalysts for electrochemical CO_2 reduction investigated with ^{18}O labeling. Angew. Chem., Int. Ed. Engl. 57, 551–554. https://doi.org/10.1002/anie.201710590.

38. De Luna, P., Quintero-Bermudez, R., Dinh, C.-T., Ross, M.B., Bushuyev, O.S., Todorović, P., Regier, T., Kelley, S.O., Yang, P., and Sargent, E.H. (2018). Catalyst electro-redeposition controls morphology and oxidation state for selective carbon dioxide reduction. Nat. Catal. *1*, 103–110.

39. Bagger, A., Ju, W., Varela, A.S., Strasser, P., and Rossmeisl, J. (2019). Electrochemical CO_2 reduction: classifying Cu facets. ACS Catal. *9*, 7894–7899.

40. Rahn, B., Wen, R., Deuchler, L., Stremme, J., Franke, A., Pehlke, E., and Magnussen, O.M. (2018). Coadsorbate-induced reversal of solid–liquid interface dynamics. Angew. Chem., Int. Ed. Engl. *57*, 6065–6068.

41. Alfantazi, A.M., Ahmed, T.M., and Tromans, D. (2009). Corrosion behavior of copper alloys in chloride media. Mater. Des. *30*, 2425–2430.

42. Van der Heide, P. (2011). Data collection and quantification. In X-Ray Photoelectron Spectroscopy (John Wiley & Sons), pp. 61–99.

43. Arán-Ais, R.M., Scholten, F., Kunze, S., Rizo, R., and Roldan Cuenya, B. (2020). The role of in situ generated morphological motifs and Cu(i) species in C_{2+} product selectivity during CO_2 pulsed electroreduction. Nat. Energy *5*, 317–325.

44. Chou, T.-C., Chang, C.-C., Yu, H.-L., Yu, W.-Y., Dong, C.-L., Velasco-Vélez, J.J., Chuang, C.-H., Chen, L.-C., Lee, J.-F., Chen, J.-M., and Wu, H.L. (2020). Controlling the oxidation state of the Cu electrode and reaction intermediates for electrochemical CO_2 reduction to ethylene. J. Am. Chem. Soc. *142*, 2857–2867.

45. Álvarez-Moreno, M., de Graaf, C., López, N., Maseras, F., Poblet, J.M., and Bo, C. (2015). Managing the computational chemistry big data problem: the iochem-bd platform. J. Chem. Inf. Model. *55*, 95–103.

46. Kresse, G., and Furthmüller, J. (1996). Efficiency of ab-initio total energy calculations for metals and semiconductors using a plane-wave basis set. Comput. Mater. Sci. *6*, 15–50.

47. Kresse, G., and Furthmüller, J. (1996). Efficient iterative schemes for ab initio total-energy calculations using a plane-wave basis set. Phys. Rev. B Condens. Matter *54*, 11169–11186.

48. Perdew, J.P., Burke, K., and Ernzerhof, M. (1996). Generalized gradient approximation made simple. Phys. Rev. Lett. *77*, 3865–3868.

49. Grimme, S. (2006). Semiempirical GGA-type density functional constructed with a long-range dispersion correction. J. Comput. Chem. *27*, 1787–1799.

50. Kresse, G., and Joubert, D. (1999). From ultrasoft pseudopotentials to the projector augmented-wave method. Phys. Rev. B *59*, 1758–1775.

51. Nørskov, J.K., Rossmeisl, J., Logadottir, A., Lindqvist, L., Kitchin, J.R., Bligaard, T., and Jónsson, H. (2004). Origin of the overpotential for oxygen reduction at a fuel-cell cathode. J. Phys. Chem. B *108*, 17886–17892.

52. Garcia-Ratés, M., and N. López, N. Multigrid-based methodology for implicit solvation models in periodic DFT. J. Chem. Theory Comput. 2016;12:1331–1341.